

PAPER

[View Article Online](#)
[View Journal](#) | [View Issue](#)

Mapping atomic motions with ultrabright electrons: towards fundamental limits in space-time resolution

Stephanie Manz,^a Albert Casandruc,^a Dongfang Zhang,^a Yinpeng Zhong,^a Rolf A. Loch,^a Alexander Marx,^a Taisuke Hasegawa,^{ab} Lai Chung Liu,^c Shima Bayesteh,^d Hossein Delsim-Hashemi,^e Matthias Hoffmann,^e Matthias Felber,^e Max Hachmann,^e Frank Mayet,^e Julian Hirscht,^a Sercan Keskin,^a Masaki Hada,^{af} Sascha W. Epp,^a Klaus Flöttmann^e and R. J. Dwayne Miller^{*acg}

Received 14th October 2014, Accepted 12th November 2014

DOI: 10.1039/c4fd00204k

The long held objective of directly observing atomic motions during the defining moments of chemistry has been achieved based on ultrabright electron sources that have given rise to a new field of atomically resolved structural dynamics. This class of experiments requires not only simultaneous sub-atomic spatial resolution with temporal resolution on the 100 femtosecond time scale but also has brightness requirements approaching single shot atomic resolution conditions. The brightness condition is in recognition that chemistry leads generally to irreversible changes in structure during the experimental conditions and that the nanoscale thin samples needed for electron structural probes pose upper limits to the available sample or “film” for atomic movies. Even in the case of reversible systems, the degree of excitation and thermal effects require the brightest sources possible for a given space-time resolution to observe the structural changes above background. Further progress in the field, particularly to the study of biological systems and solution reaction chemistry, requires increased brightness and spatial coherence, as well as an ability to tune the electron scattering cross-section to meet sample constraints. The electron bunch density or intensity depends directly on the magnitude of the extraction field for photoemitted electron sources and electron

^aThe Max Planck Institute for the Structure and Dynamics of Matter, Center for Free Electron Laser Science, Luruper Chaussee 149, Hamburg 22761, Germany. E-mail: dwayne.miller@mpsd.mpg.de

^bDepartment of Chemical Engineering, Faculty of Engineering Kyoto University Katsura, Nishikyo-ku, Kyoto, 615-8510, Japan

^cDepartments of Chemistry and Physics, University of Toronto, Toronto, Ontario M5S 3H6, Canada

^dInstitut für Experimentalphysik, Universität Hamburg, Luruper Chaussee 149, Hamburg 22761, Germany

^eDESY, Notkestrasse 85, 22607 Hamburg, Germany

^fMaterials & Structures Laboratory, Tokyo Institute of Technology, Japan & JST-PRESTO, Yokohama 226-8503, Kawaguchi 332-0012, Japan

^gThe Hamburg Centre for Ultrafast Imaging CUI, Universität Hamburg, Luruper Chaussee 149, Hamburg 22761, Germany

energy distribution in the transverse and longitudinal planes of electron propagation. This work examines the fundamental limits to optimizing these parameters based on relativistic electron sources using re-bunching cavity concepts that are now capable of achieving 10 femtosecond time scale resolution to capture the fastest nuclear motions. This analysis is given for both diffraction and real space imaging of structural dynamics in which there are several orders of magnitude higher space-time resolution with diffraction methods. The first experimental results from the Relativistic Electron Gun for Atomic Exploration (REGAE) are given that show the significantly reduced multiple electron scattering problem in this regime, which opens up micron scale systems, notably solution phase chemistry, to atomically resolved structural dynamics.

1 Introduction

One of the long standing objectives in science has been to have sufficient spatial and temporal resolution to directly watch atomic motions during the primary motions governing structural transitions.^{1,2} This quest is relevant to helping understand at the atomic level of detail, effectively, all classes of structural transitions from issues of condensed matter physics of strongly correlated electron-lattice materials, extreme states of matter, and biological functions. In chemistry, this objective is central to the discipline. The very notion of a chemical process involves the passage of a system from one stable structure to another in which the chemist tries to control conditions to direct the desired process over the myriad of other possible outcomes. The ability to control chemistry largely resides in arranging conditions to lower the barrier and entropic factors to favour a particular chemical pathway. The intellectual pursuit of chemistry is to understand the factors that control barrier heights, within the context of a complex many body potential, and to connect molecular structure to macroscopic properties. This statement is intended to include advances in *ab initio* theory, synthetic strategies, and experimental methods to probe different aspects of the system and system-bath interactions driving chemistry. The unifying concept in this pursuit is to try to identify the key atomic motions that lead the system over the barrier region, or stated differently to picture the transition state region, the critical “point of no return” that connects the reactant to the product free energy surfaces. A direct observation of atomic motions during the transition from one structure to another would provide the most rigorous test possible for various concepts that have evolved for inferring chemical pathways. We could see this directly. This objective has now been met.^{3–5} The recent development of ultrabright electron and X-ray sources to provide the necessary structural probes have opened up the femtosecond time domain to atomically resolved dynamics.^{2–8} The source technology is rapidly advancing to enable atomic imaging of structural dynamics of ever larger and more complex systems. There are, however, fundamental limits to source brightness and sample issues that need to be overcome to apply this new imaging modality to problems of general interest.

For the purpose of this discussion, we will focus on source requirements with respect to spatial and temporal resolving power to study molecular systems undergoing chemical reactions. In regard to time resolution, the relevant time scales to this problem have been well appreciated since the first connection of microscopic processes to reaction rates in the quest for an absolute rate theory.⁹

This work ultimately led to the development of transition state theory. The defining moment of chemistry is captured in the discussion of barrier crossing processes. This time scale varies for different systems but is on the order of few 10 s of femtoseconds (fs; $1 \text{ fs} = 10^{-15} \text{ s}$) to 100 femtosecond time scales. There are faster motions in nature. For example, the OH stretch of water has a period of 10 fs but the motions involved are less than 0.05 \AA , hardly chemically relevant. The time scale is defined by the relevant motions over length scales corresponding to 0.1 to 1 \AA , leading to distinct changes in structure. More specifically, these motions must in turn be coupled to the nuclear continuum of states to relax the system to a displaced minimum in the many body potential corresponding to a long lived state or stable product state. There must be damping or energy dissipation in the process to relax on the product surface. It is the approximately 100 fs time scale of relaxation along a reaction coordinate that dictates the required time resolution. It is important to realize that not all motions are equally coupled to the reaction coordinate and the degree of coupling rapidly evolves in the barrier crossing region.⁴ The highly anharmonic nature of the many body interactions at this far from equilibrium point in nuclear configuration space leads to strong mixing of the otherwise suitable normal mode basis to describe equilibrium fluctuations. Normal modes are accurate descriptions of atomic motions for small excursions over which the potential is well approximated to be harmonic, *i.e.* the nuclear fluctuations are within linear response limits. The far from equilibrium fluctuations that sample the barrier crossing region are highly nonlinear and the most anharmonic modes tend to be the low frequency modes that undergo the largest relative motions. These modes are also the most highly damped as they occur within the highest spectral density of modes for conserving energy and momentum in the relaxation process.^{10,11} It is the net excursion along the modes most strongly coupled to the reaction coordinate that define the relevant time scales of chemistry. These modes, whether involving intramolecular processes, solvent controlled chemistry, or the chemistry controlled by protein environmental fluctuations, tend to be in approximately the 100 cm^{-1} frequency range, which gives rise to the generalized requirement of 100 fs time resolution to capture the chemistry.⁴

The spatial resolution requirements are equally challenging in that one needs sub- \AA spatial resolution to pull out the important relative motions directing atomic displacements from one stable structure to another. To a first approximation, the spatial resolution requirement exceeds that needed for static structure determination. For example, in the photo-isomerization of retinal, the primary event involved in vision and energy transduction within the rhodopsin family of proteins, the key motions are on the order of 0.1 \AA for the carbon atoms at the central bond axis of the isomerization.¹² Save in the act of bond dissociation, chemically relevant motions are between 0.1 and 1 \AA . To fully resolve the primary motions requires either hard X-rays or high energy electron probes with sufficiently short carrier wavelengths to resolve these motions. Even so, this level of spatial resolution would be out of range for most sources, however, time-resolved measurements involve differential measurements. The initial structure is known. It is only the relative changes from this known starting point that need to be resolved, not the entire structure for every atomic position to this level of accuracy. The key to being able to resolve chemically relevant motions is that the source serving as the structural probe must be sufficiently stable and bright

enough to render signal to noise ratios (SNR) sufficient to pull out these small relative changes in intensity that report the atomic positions. The most sensitive method for determining atomic structure is the use of diffraction methods or imaging in reciprocal space. This observable takes advantage of the N^2 amplification of the diffracted signal intensity by scattering off N identically arranged molecules to amplify the scattered signal. The criteria of high brightness and high stability for the source reduce to achieving sufficient signal to noise ratios in the diffracted orders to pull out the structural changes of interest. The quality of sample often plays a deciding factor in the achievable resolution; however, it is only recently that the sources serving as structural probes have reached the level of brightness where sample issues are the main bottleneck.

Differential detection of the structural changes is achieved by comparing the changes in structure following an excitation pulse, which triggers the structural change of interest. Here, it needs to be fully appreciated that, in the absence of a “trigger”, the act of barrier crossing driven by background thermal noise is a rare event. For even small barriers (e.g. 1 eV), there are less than $1 : 10^8$ molecules undergoing a barrier crossing event at any instant in time.⁴ In principle, one could track the motions of an individual molecule undergoing first order reactions, or molecular collision partners for second order processes, to observe such crossings but the ability to observe such motions and the enormity of collecting sufficient atomic images at the required framing rate to get above background noise, never mind increased demands on source brightness, make this prospect intractable. The processes of interest must be optically triggered to observe the key relative atomic motions connecting two stable structures within the complex, highly dimensional, potential energy surfaces of interest to chemistry. This simple realization has a number of important consequences for the conduct of the experiment. First, the perturbation used to trigger the chemistry must be faster than the ensuing motions of interest. Only femtosecond laser excitation meets this requirement. Furthermore the optical excitation must prepare the system on excited state surfaces that intersect reactive crossings under barrierless conditions. If there is a barrier in the excited state, the time scale for the buildup of the product state is much slower than that of the primary motions involved. In the presence of a barrier, the system will reach a thermal equilibrium within the vibrational modes corresponding to the excited state surface. In this event, there are uncorrelated, thermally, sampled crossings and the details of the relevant motions will not be resolved. The problem reverts to the same statistics as trying to capture barrier crossing events along the ground state. This requirement for an effectively barrierless excited state process not only limits the number of potentially tractable systems for study but has additional consequences. To observe the relevant motions above the background of unexcited molecules requires that on the order of 10% of the molecules or lattice sites are undergoing the photoinduced structural change. The quantum yield for the desired photo-process must be at least this large and there is an upper limit to the degree of excitation. The <100 femtosecond requirements for the excitation pulse necessarily leads to high peak powers, however, the peak power must be maintained at excitation levels on the order of 100 GW cm^{-2} or lower to avoid multi photon ionization artifacts.¹³ Basically, above this peak power multi photon processes begin to dominate and even the degree of state preparation becomes ill defined as multi photon excitation to higher lying excited states begin to also significantly contribute. For typical

molecular densities, this latter condition means that samples must be on the order of a few microns or thinner or else the required excitation levels (>10% photoproduct formation) lead to excessively high incident peak powers. These are nontrivial sample constraints as one must have sufficient surface area within this thickness restriction to attain adequate signal to noise to stitch together a movie of the atomic motions involved in the process of interest.

Of all the above discussed requirements, the most limiting is the requirement for approximately 10% of the system to be undergoing the phototriggered structural transition. Apart from gas phase systems, which can be rapidly exchanged between laser shots, this level of excitation leads to sample damage in a single shot. This statement is especially true for single crystals that give the highest structural resolution. Normally in diffraction experiments, the upper limit for source brightness is determined by X-ray or electron induced damage. In this class of experiments, the main limitation with respect to sample damage is not the structural probe but the excitation process to trigger the chemistry that damages the sample. It is not enough to have simultaneous atomic resolution with 100 fs time resolution or less but one must attain this experimental parameter space within single shot conditions. Herein lies the real challenge. The source brightness for the structural probe must not only be capable of high space-time resolution but of sufficient intensity to achieve atomic resolution at or approaching single shot conditions.^{4,14}

Enormous gains in source brightness have been achieved for both electron and X-ray sources to meet this condition. The major advance in X-ray source brightness was achieved through technical advances made in undulator technology that enabled scaling the free-electron laser concept to the X-ray range. These sources are referred to as 4th generation light sources or X-Ray Free Electron Lasers (XFELs). In comparison to 3rd generation synchrotron sources, XFELs represent an increase in source brightness of over almost ten orders of magnitude.⁷ XFELs are not true laser resonators but are based on self amplification of spontaneous emission or SASE sources. As with SASE sources in the visible range, there are huge stochastic fluctuations in intensity and spectrum that make shot to shot normalizing essential to improve the SNR. In addition, there are time jitter issues, with respect to synchronizing the laser excitation used to trigger structural changes and the RF phase of the electron acceleration, that gives rise to 200 fs timing jitter. In principle, XFELs are capable of <50 fs time resolution using time stamping methods as another normalization step to extract the time dependent changes in diffraction efficiency.¹⁵ To date, time-resolved structural dynamics on the prerequisite time scales (100 fs to picosecond) have not been realized with sufficient numbers of diffraction orders to follow structural changes. There has been a recent report of resolved structural changes, albeit not the actual transient structures, on the microsecond time scale¹⁶ and studies of a single diffraction order have been used to infer the role of the lattice in directing material properties for strongly correlated electron lattice systems.¹⁷ There remain a number of technical challenges in the normalization procedures required to attain sufficient SNR and also in the large number of crystal projections needed for X-ray structure determination, prior to the onset of X-ray induced damage, that have hindered efforts in this direction. Further, these sources are not dedicated facilities to this line of inquiry. The most important application for XFELs appears to be in the use of the high spatial coherence and brightness to enable nano- to micro-protein

crystallography, prior to the onset of X-ray induced damage.⁸ Recent developments in self-assembly of up to M-pixel crystal arrays or photochips^{18,19} (solid target solution to sample delivery) and aerosol injectors to give random orientations²⁰ may solve the last technical obstacle in providing a general solution for collecting sufficient reciprocal space to stitch together atomic movies on the femtosecond time scale.

With respect to electron sources, there are inherent electron–electron repulsion or space charge effects that limit source brightness. This problem was readily appreciated and it was felt that it would not be possible to achieve the needed brightness with electron sources. In this regard, there have been proposals to achieve the necessary space-time resolution with low intensity sources, with single electron pulses being the ultimate limit to completely avoid space charge limits in time resolution.^{21,22} The basic problem is that one needs approximately 10^5 to 10^6 electrons to have sufficient SNR to invert diffraction patterns to structures and approximately 2–3 orders of magnitude more for real space imaging. In the single electron limit, this requirement translates to over 10^8 photoexcitation events in the data collection process. It is not possible to have sufficient sample area for such a large number of excitation events, save for gas phase samples where other issues have limited the time resolution. One needs fully reversible systems that can withstand over 10^6 photocycles between reactive excited and ground electronic states. The prospect of using single electrons remains an elusive prospect with respect to achieving simultaneous femtosecond time resolution and sub-Å spatial resolution to structural transitions. To date, there has only been one report on time resolved dynamics in the single electron limit in which simple thermally excited acoustic phonons were followed on the 100 ps timescale. This process is fully reversible by its very nature as it does not involve a structural change. This work rather reinforces the importance of brightness. In all cases, the brighter the source the better the space-time resolution is, as long as the time resolution is sufficient to follow the dynamics of interest. As will be seen below, ultrabright electron pulses on the order of 10 fs are now possible, which provides sufficient time resolution to follow even the fastest nuclear motions. The first atomic movie with sufficient space-time resolution, *i.e.*, sufficient number of diffraction orders, to resolve the relative atomic motions involved in a structural change was in fact captured with a high brightness electron source.³ The major advance that made this possible was the realization that high bunch charge electron pulses do not lose space-time correlation at sufficient intensities to achieve single shot structure determination. This realization was made possible through an effectively exact solution to the electron propagation dynamics by solving the coupled equations of motions of some 10^4 electrons,²³ sufficient for the structure determination of systems with simple unit cells (<3 nm). It was discovered that the transverse velocity spread, related to the transverse spatial coherence, was not significantly affected. The main issue was the longitudinal space charge effect. Two solutions were apparent from these calculations. One solution involved the use of extremely short propagation paths to the sample target to limit pulse broadening to retain 100 fs time resolution. Here, the key realization was that the transverse coherence, even at short propagation distances with typical transverse velocity spreads, was sufficient for atomic resolution for systems with unit cells of a few nm. The other solution to emerge from this work was to explicitly exploit the conserved space-time

correlation and development of an extremely linear chirp that naturally develops for nonrelativistic electrons to compress the pulse at the sample position. In this respect, the electrons at the front of the electron pulse experience electron–electron repulsion effects that lead to acceleration or energy exchange between the electrons at the back of the pulse that experience deceleration. For nonrelativistic electrons, the higher energy electrons travel faster than the slow energy electrons. The electrons at the front stay at the front and the electrons at the back stay at the back to conserve the original space-time relationship and develop an extremely linear chirp with propagation. This observation led to the proposal for the use of electric field compression methods or other dispersive elements to compress the electron pulse.²³ The use of a longitudinal half cycle RF cavity to recompress the pulse conserves the transverse coherence and appears to be the best solution to pulse compression for high brightness applications,²⁴ although there are other applications for improved time resolution.²⁵ The overall gains in electron source brightness over previous low electron density pulsed sources approaches similar gains as XFELs over prior technology. The compact electron gun design is now capable of 10^5 to 10^6 electrons per pulse in a 200 fs pulse that is focusable down to 100 micron radius spot sizes typically used in femtosecond laser experiments.² New designs at higher energies will enable <100 fs pulses. The DC-RF pulse compression concept has achieved approximately a factor of 10 increase in brightness with attendant technical issues in RF timing jitter that currently limit the achieved time resolution to approximately 200 fs.^{2,26–28} The time resolution can be improved to 30 fs with the use of time stamping methods.²⁹ In comparison, the compact electron gun is jitter free. These table top electron sources are exceptionally bright. For calibration, taking into account the factor of 10^5 to 10^6 higher scattering cross-section for electrons over X-rays for the same energy, this source technology is comparable to 10^{12} X-ray photons per pulse for practical laser excitation parameters, *i.e.* these electron sources are on par with XFELs in terms of observed signal levels. Here it is important to keep in mind that peak power limitations require the use of samples on the micron scale or smaller such that there is little distinguishing differences in sample requirements. The diffraction efficiency for X-rays is very small for sample thicknesses on the micron scale such that the observed signal levels are expected to be similar for these two different source technologies. The big differences are that the electron sources are dedicated table top facilities for this class of experiment and are orders of magnitude more stable than the X-ray counterpart. It is these decided advantages that has enabled atomic movies of the primary motions involved in structural transitions to be first captured using electron sources. Advances in laser generated X-ray plasma sources have likewise opened up atomically resolved structural dynamics on the prerequisite sub-ps timescale.^{30–32} The most important difference in brightness levels of XFELs sources in relation to all other sources is the near perfect transverse coherence. This difference makes XFELs the ideal source for the study of complex large unit cell systems such as proteins; whereas electron sources are currently limited to transverse coherences suitable for the study of relatively small systems (<10 nm unit cells). This difference may not hold for long, as will be discussed in this report. Electron sources have at least 2 orders of magnitude possible increase in brightness that may close this gap in imaging resolution. In this respect, the recent introduction of relativistic electron sources for this application^{33–38} promises to provide the highest spatial-temporal

resolution due to the reduction of pulse broadening effects in the relativistic regime. The full potential of relativistic electron sources to achieve the highest possible time resolution relies on removing the initial velocity and temporal spread in the RF acceleration phase. This discussion paper focuses on the first results from the Relativistic Electron Gun for Atomic Exploration (REGAE) that introduces the use of a rebuncher cavity to achieve the ultimate limit in high brightness for relativistic electron sources.

2 Ultrafast diffraction and real space imaging with relativistic electrons

2.1 Coherence issues: diffraction

The focus of this discussion paper is on electron source technology for atomic imaging dynamics on the primary time scales of chemistry. The image resolution as with any source is related to both the transverse and spatial coherence of the source for diffractive imaging or aberrations in the lens system for real space reconstruction. For X-rays or other light sources, the degree of coherence is defined by the beam divergence, which is a constant after the modality of light generation is fixed. For electrons, the degrees of transverse and longitudinal coherence are coupled parameters that depend on the specific space-time focusing. As an electron pulse is made shorter in duration for a given bunch charge at some point the space charge effects and spatial inhomogeneity will lead to increased beam divergence or transverse velocity spread and corresponding loss of in-plane resolution. The transverse spatial coherence is defined by:^{39–41}

$$L_x \approx \lambda/2\pi\sigma_\theta \approx \hbar/\sigma_{p_x}, \quad (1)$$

where σ_{p_z} is the angular spread, and σ_{p_x} is given by the transverse momentum spread. There is a similar relation for the longitudinal coherence, which is defined as:

$$L_z \approx \hbar/\sigma_{p_z}. \quad (2)$$

The longitudinal coherence is only an issue if one wants to coherently reconstruct an image as in holography. For diffractive imaging, the longitudinal coherence is not the limiting factor. The coherence length, even for strongly space charge broadened pulses, is generally much larger than the unit cells of even large unit cell crystals (>10 nm). Thus, the two most important, coupled, parameters to consider in attaining the required space-time resolution for a particular problem of interest is to match the transverse coherence to the unit cell of interest for the spatial resolution and to adjust the electron bunch density accordingly to give the required electron pulse duration for the desired time resolution. In the former case, the required spatial resolution is achieved by adjusting the source size at the photocathode or introducing an aperture to produce an effective source size that gives a transverse coherence length at the sample position that is a few times the lateral dimension of the unit cell.⁴¹ In terms of time resolution, the required spatial resolution limits the bunch density for a given transverse energy spread and the minimum pulse duration on target is achieved by reducing the number of electrons for a given probe beam size at the sample position, until the

longitudinal space charge effects are negligible relative to the time resolution needed. Again, these parameters are coupled.

For most problems of chemical interest, the pulse duration with sufficient electrons for single shot structure determination is the primary concern. The shortest electron pulses are achieved with the highest extraction fields as this minimizes the pulse propagation time to the sample position and thereby minimizes space charge broadening of the time resolution. The highest extraction fields are achieved with RF acceleration methods that avoid charge accumulation and breakdown. Extraction fields an order of magnitude larger than DC electron guns are possible. In addition, as one goes to higher electron energies, there is a reduction in space charge broadening due to the relativistic correction to the electron velocities. To first order, in the relativistic regime, all the electrons would travel at essentially the same velocity, near the speed of light. In this limit, the time broadening problem would reduce solely to issues related to the transverse coherence or transverse velocity spread that would increase with temporal compression in the longitudinal direction. What are the fundamental limits to space-time resolution with electrons? There are new developments both in the generation of ultrabright electrons sources for the shortest possible electron pulse durations/temporal resolution and photocathode concepts that promise to offer orders of magnitude increases in transverse coherence. These higher energy electron sources also have greater penetration depths to greatly reduce sample constraints. We are entering into a new regime for electron sources. The order of magnitude higher field gradients possible with relativistic electron guns and enormous reduction of longitudinal space charge broadening in the relativistic regime hold promise to provide the brightest sources possible for the highest possible spatial-temporal resolution. We highlight the promise to go beyond present limits in diffraction or reciprocal space imaging of chemical and biological problems – for which the dynamics are essential to understanding mechanism and functionality.

2.2 Coherence issues: real space imaging – dynamic high energy electron microscopy

The incoherent nature of the spatial phase of the electron pulses across the beam profile presents more difficulties for real space imaging than for diffraction, that are hard to compensate. To acquire an image with reasonable signal to noise ratio at the detector position, one aims for 10^6 to 10^7 electrons per acquisition, which needs to be matched to a typical sample area of a few μm^2 . The electron beam needs to be tightly focused to achieve this density. A tight focus on the other hand means a reduction of the local coherence length, which calls for an improved total coherence of the electron pulse from its source on. The photoemitted electron image at the cathode has to be as close to point-like as possible. Laser spot sizes below $10\text{ }\mu\text{m}$ are difficult to achieve at the cathode position inside an RF cavity. Typically, the laser is coupled into the cavity from a window several tens of cm away from the cathode surface, which is insufficient working distance to focus tighter than $10\text{ }\mu\text{m}$. It is possible to use structured cathodes to give the desired source size. However, for current designs, single shot imaging will only be possible with a partially coherent mode and thus relies on Z -contrast (Z = atomic number) rather than phase contrast. By spatial filtering with an aperture, the

scattered electrons lead to an intensity drop in the imaged electron beam relative to the position of the scattered object for bright-field imaging. In dark field imaging, the unscattered electron beam is stopped by a negative aperture (beam stop) and the scattered electrons are imaged. In both cases, the favorable situation is for each electron to scatter less than once on average. Too little scattering gives low imaging contrast and calls for high electron doses, whereas multiple scattering broadens the minimal spot size of point scatterers in the sample. The number of scattering events depends on the elastic cross-section σ_{el} , which depends on the electrons' energy and the atomic number Z of the scattering material. An approximate expression for σ_{el} is given by:⁴³

$$\sigma_{\text{el}} = \frac{c^2 h^2 Z^{4/3}}{\pi E_0 \beta}, \quad (3)$$

where E_0 is the electron rest energy, and $\beta = v/c$ with the electron's velocity v . The mean free path Λ_{el} of an electron in a material with density ρ is related to the cross-section by $\Lambda_{\text{el}} = A/N_{\text{a}}\sigma_{\text{el}}\rho$. While the expression for σ_{el} gives a helpful approximation, it can differ from the actual cross-section by a factor of 2. We use the approach presented in ref. 42 to include relativistic corrections in the calculation. In Fig. 1, we compare calculations for the elastic cross-section using the Schrödinger equation, the relativistically corrected Schrödinger equation, as well as the Dirac equation. Solvers for both the relativistic Schrödinger equation and Dirac equation have been implemented into the EDICo-code.⁴⁴ The calculations were performed for unpolarized electrons. We find no significant difference between the relativistic Schrödinger and Dirac result and conclude that effects of spin can be neglected, as also stated in ref. 42. In terms of beam propagation

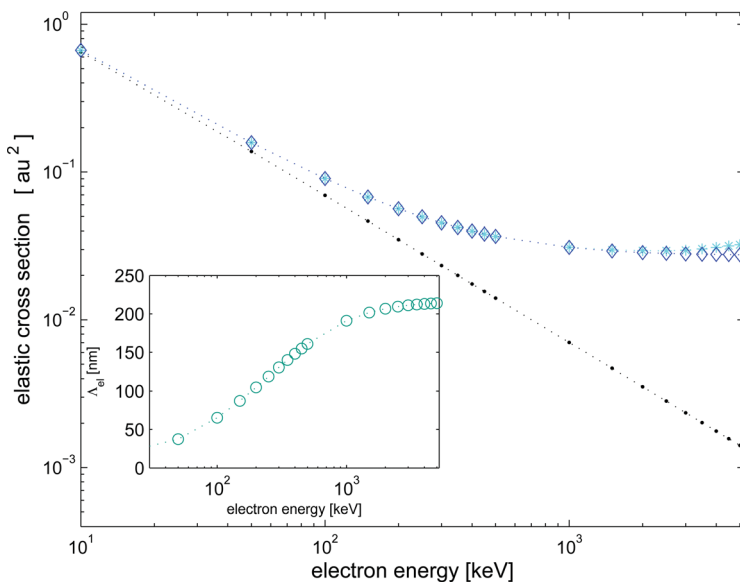


Fig. 1 Comparison of different methods to calculate electron cross-sections in aluminum using the relations given in ref. 42. The inset shows the according mean free path in aluminum for the cross-sections derived from the Dirac equation.

through the sample and effect on imaging, the electron beam broadens its energy distribution in the sample by inelastic collisions. Typically, the total cross-sections for elastic and inelastic scattering show a qualitatively similar behavior with energy. The ratio $\eta = \sigma_{\text{inel}}/\sigma_{\text{el}}$ was experimentally found to be $\eta = 20/Z^{45}$ and theoretically $\eta = 26/Z$.⁴³ Since the cross-section for elastic and inelastic scattering follow similar behavior with energy, η is almost constant in the keV to MeV range. One can assume that multiple scattering will be reduced by the same factor for both elastic and inelastic scattering. Damage due to ionization will also be reduced by the same argument, but knock-on damage will be more severe than for lower energy devices.

When the sample thickness exceeds the mean free path in the material, one faces two problems in transmission electron microscopy that stem from multiple scattering: multiple elastic scattering increases the minimal spot size of a point like object; and inelastic scattering similarly leads to aberrations in the reconstructed real space image. Thus, the resolution will be reduced and distorted. Such effects are reduced in electron microscopy with relativistic electrons, and allow in the case of light, low Z , organic materials, the study of micron thick samples with nanometer resolution. High resolution microscopy with thin samples in which atomic resolution is desired may better be performed in conventional electron microscopes employing aberration correctors⁴⁶ that are not currently available for relativistic electron imaging systems.

We studied the feasibility of dynamic real space imaging with pulse propagation simulations in ASTRA. The simulation is launched from the sample position on. A pulse of 10^4 particles with a Gaussian density profile and an energy of 3 MeV is tracked through the magnetic field of a realistic electromagnetic solenoid, which is a likely implementation for the objective lens. The solenoid field was calculated using the CST software suite.⁴⁷ A schematic of the imaging system implemented in the existing REGAE setup is shown in Fig. 2(a). With the pulse, 500 test particles were used to probe the mean field space charge that travel along the propagation direction. For a chosen spot size of 10 μm at the sample, the test particles travel off-center at a distance of 1 μm . The relative energy spread for the pulse is chosen to be 2×10^{-4} . The transverse momentum spread of the test particles was chosen to match scattered electrons up to typical angles of 5 mrad. We performed the simulation for three different focal lengths of 1.1 cm, 5 cm, and 10 cm. The results depending on the bunch charge are presented in Fig. 2(b). We tracked the test particles until they reached the image plane, and then computed the RMS width to obtain a point spread function. We find higher resolution for lower focal lengths, which is to be expected from the respective spherical aberration coefficients. Furthermore, we observe a decrease in resolution depending on charge, which we interpret as the result of the inhomogeneous space charge field in the bunch, an effect resembling spherical aberrations.⁴⁸ The simulation has been repeated for different pulse lengths and spot sizes. We find a similar scaling for all pulse shapes, as visible in Fig. 2(b). In order to reach 1 nm resolution the charge must be kept in the fC range. Longer pulses would certainly relax the issue of space charge induced aberration, as proposed in,^{49,50} but then additional, higher harmonic cavities need to be employed to decrease the energy spread that comes with the generation of a long pulse in an RF cavity, which has not been treated in these works.

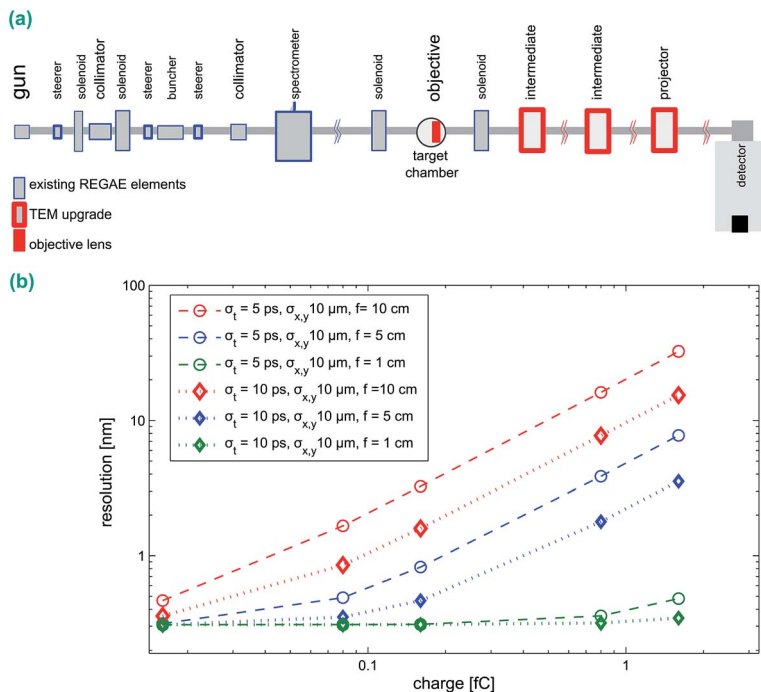


Fig. 2 (a) Schematic of the implementation of a TEM mode within the existing REGAE setup. (b) Effect of charge and objective focal length on resolution for a pulse length of 5 and 10 ps. The beam shape is Gaussian for all cases.

2.3 Electron diffraction with REGAE

2.3.1 The REGAE apparatus. The relativistic electron gun for atomic exploration, REGAE, is a radio frequency (RF) accelerator based gun design operating in a pulsed mode with 50 bursts per second. It is mainly dedicated to the study of structural dynamics in solid, liquid and gas phase of organic and inorganic samples. As elucidated in the introduction, such a device has to fulfill the requirements of short pulses, high brightness, and high coherence at the same time. Electron pulses are created *via* photoemission by 266 nm, 500 fs pulses of a frequency-tripled Ti:Sa laser impinging the cathode within a 1.5 cell S-band cavity. For the studies presented here, we use either molybdenum, gold, or Cs₂Te as the cathode material. By means of a coaxial on-axis coupler, a travelling 3 GHz S-band wave of some micro-second length launched by a klystron is fed in resonance into the gun cavity, where field gradients of up to 100 MV m⁻¹ can be obtained leading to electron energies up to 5 MeV. Running the cavity at high fields has, apart from the beam energy itself, the major advantage that high bunch charge densities can be extracted from the cathode overcoming conventional space charge limitations. Depending on the cathode material and its quantum efficiency, bunch charges in the range from pC for gold and other metal cathodes and 10 pC for Cs₂Te can be extracted. For typical diffraction experiments, we aim for a bunch charge of 100–200 fC (about 1 million electrons) at the target position, as a compromise between beam quality and signal strength. The elements of the beamline are depicted in

Fig. 3. The gun section is followed by electro-magnetic solenoids and collimators to shape the beam. The collimators are a critical feature and require a high degree of engineering to ensure proper alignment under the ultrahigh vacuum conditions needed to run the RF cavity. These elements are used for collimation and beam clean up as well as to reduce dark current travelling in the beam direction. One of the most important distinctions of this relativistic electron gun is the low dark current⁵¹ that is primarily due to the very low base pressure of 10^{-10} mbar employed in this design concept. Additional beam diagnostic stations allow for determination of transverse electron bunch parameters, *e.g.* beam width, energy, and energy spread. The beam charge can be detected without disturbing the beam by means of a resonator, where the electron pulse induces a TM01 mode at 1.3 GHz. The bunch charge can be measured with fC resolution.⁵² The other key feature to this design is the introduction of a rebunching cavity to obtain the shortest possible pulses at the sample position. The design employs the same klystron amplifier with an RF splitter to drive both cavities, which requires finding unique phase solutions for which the pulse is optimally compressed for a given amplification. The rebunching cavity is designed to temporally refocus the electron pulse at a distance of 5.5 m from the photocathode position. For detection, a scintillator on a fiber optics plate in the beam line converts the electrons' density distribution to photons, which are coupled to an EMCCD chip outside of vacuum. The high dynamic range of the EMCCD combined with its high sensitivity down to single electron detection allows for simultaneous detection of the undiffracted beam and diffraction patterns without the necessity for a beam block (Fig. 4).

2.3.2 Beam dynamics and time resolution at REGAE. The beam dynamics after the gun are controlled by solenoid magnets, indicated by arrows in Fig. 3. Depending on the demands on beam size at the sample position and extent of the diffraction pattern on the detector screen, we either focus the beam through the target on the screen with solenoid lenses (see Fig. 3), or – if a higher intensity at the target is called for – have a small spot at the sample and refocus on the detector position. Ideal beam dynamics for diffraction in terms of a phase advance⁵³ approaching 90° has been found only without an intermediate focus.

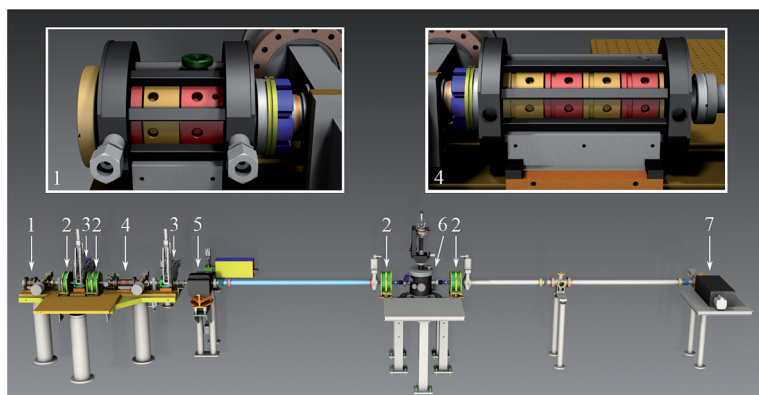


Fig. 3 REGAE scheme. Indicated with numbers are: (1) gun cavity, (2) solenoids, (3) collimators, (4) rebunching cavity, (5) dipole for electron energy measurements, (6) target interaction chamber, and (7) detector.

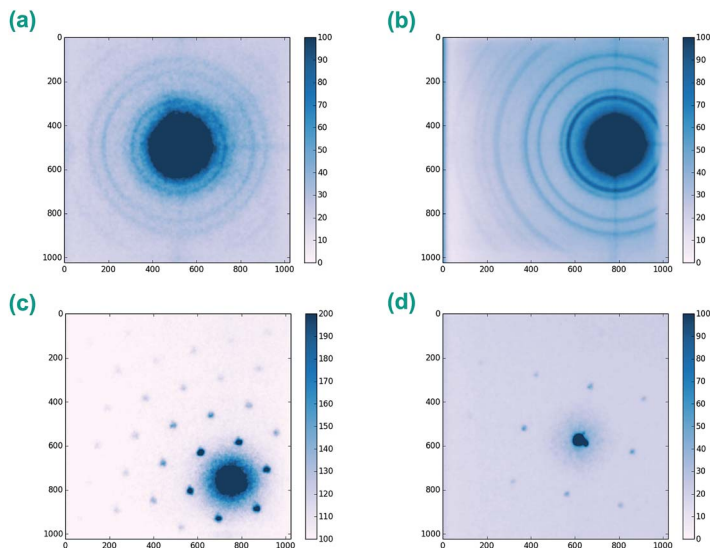


Fig. 4 Example diffraction patterns from (a, b): polycrystalline gold, (c): MoS₂, (d): Si; the quality of the diffraction is particularly notable for the single crystal samples MoS₂ and Si.

Beam size, divergence, and coherence are controlled by the photocathode and gun cavity, and transverse beam shaping elements, as solenoids, collimators and steerers. At a distance of 1.3 m from the accelerator, a rebunching cavity is placed in the beam line. It consists of four cells and is operated off-crest compared to the arrival time of the electron bunch. The rebunching cavity is driven by a fraction of the RF field that also supplies the gun. The relative phase between the cavities is adjusted with phase shifters. While the parameter space of this coupled cavity system is finite, efforts have to be made to overcome complications due to reflections and unwanted feedback between the two coupled cavities.⁵⁴ The electron bunch can, if higher acceleration is required, also be injected on-crest into the rebunching cavity. Potential beam parameters along the propagation axis are summarized in Fig. 5. For this example, the beam dynamics for a bunch of 100 fC is tracked by the ASTRA⁵⁵ simulation software, which includes space charge fields. For the initial beam parameters, we use an RMS spot size of the laser at the cathode of 10 μm , a pulse length of 0.5 ps and a charge of 100 fC. For this charge, the beam size at the target reaches 500 μm with a transverse coherence length above 10 nm. With the buncher tuned to the appropriate phase, a bunch length of 10 fs can be expected at the longitudinal focus at the sample position. We then use a solenoid close to the sample position to focus the beam and diffraction pattern to the detector. It needs to be emphasized that a pulse duration of 10 fs is sufficiently short to capture even the fastest possible nuclear motions involved in chemical processes. The achievable transverse coherence is also notable in that the design objectives were to provide sufficient transverse coherence to enable the study of systems as large as proteins. The unit cell of protein systems capable of being phototriggered to execute their biological functions such as heme proteins and the family of rhodopsin photoactive systems are on the order of 6 nm such that the transverse coherence is sufficient for this purpose.

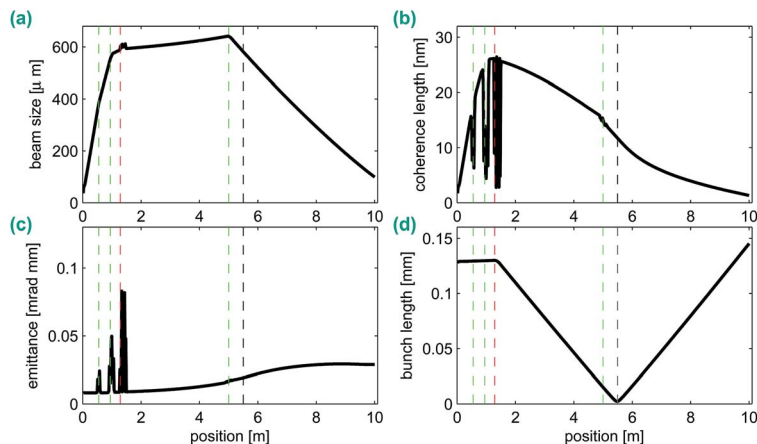


Fig. 5 ASTRA simulations for diffraction with REGAE: (a) RMS beam size showing the beam dynamics, (b) transverse coherence length, (c) emittance, and (d) bunch length in mm, corresponding to 10 fs at the longitudinal focus. The dashed lines indicate the position of solenoids (green), the rebunching cavity (red) and the sample position (black).

2.4 Static diffraction from aluminum: thickness dependence

One of the main limitations in the use of electron structural probes is the effect of multiple scattering due to the intrinsically high scattering cross-section of electrons. The increased electron penetration depth and reduced scattering angles for relativistic electrons promise the feasibility of ultra-fast electron diffraction (UED) with thick samples. In conventional electron microscopes and electron guns at intermediate energies (DC guns) typical sample thicknesses range from few tens of nanometers to 200 nm, depending on the density and atomic weight of the material. However, many interesting systems, such as protein crystals, water soluble crystalline systems, and solution phase chemistry call for a probe with a higher penetration depth. From the point of view of material science, a higher penetration depth supports the study of bulk properties with minimal effects from interfaces or surface effects. The relativistic electron energy regime has not been extensively studied and, as discussed above, only approximate relationships in terms of scaling relations for elastic and inelastic scattering are available. The effect of multiple electron scattering on image resolution needs to be explicitly determined. We explored these possibilities using films of polycrystalline aluminum of increasing thickness up to 800 nm. The calculated mean free path according to the inset in Fig. 1 is just above 200 nm. The films are supported by a 30 nm thin SiN membrane. Diffraction patterns were recorded by integrating 300 shots of 180 fC pulses at 4 MeV. Before azimuthal integration of the diffraction pattern a background image is subtracted. The incoherent contribution and the diffuse diffraction ring from the SiN membrane are modeled with a multi-component function and removed as well. These components are shown as gray lines in Fig. 6(a). The off-center peak at about 0.78 \AA^{-1} corresponds to diffuse diffraction from the supporting SiN membrane. We need to determine the effect of multiple electron scattering as a function of thickness for a given system and use the Z dependence of the scattering to provide general guidelines for limiting

this effect on reciprocal (diffraction) or real space resolution. Coherently scattered electrons interfere after multiple elastic scattering, thus, the diffracted intensities are altered compared to the single scattering regime. Inelastic scattering leads to a broadening of both probe beam and diffracted electrons and can affect the resolution. The addition of both effects is visible as an increase of diffraction ring width, as shown in Fig. 7(c). The question whether multi-scattering effects are necessary to describe such diffraction patterns in theoretical treatments or the degree to which structural information is lost are still open. Modulations in diffraction intensity might be averaged out in polycrystalline samples, as expected from multi-slice calculations. To aid in resolving this issue, we compare the ratio of diffraction intensities for different rings in Fig. 7(a) with the expected result for a completely random powder sample, obtained from the software CrystalMaker.⁵⁶ The rather surprising result is that the multiple electron scattering effects, while occurring, are not significantly altering the relative ratios of the different diffraction orders as needed for dynamic structure determination. The small deviation from ideal results is within signal to noise limits for some of the diffraction orders. To be fully conclusive, the effect of substructure, grain size and texture within the polycrystalline sample would need to be studied by a different method.

This study gives a direct determination of the effect of multiple electron scattering on a well-defined system. In the present case, Al is close in Z to organic systems. We conclude that time-resolved electron diffraction studies of systems, at least for light materials, is possible up to micrometer thickness in the relativistic energy range. Here is especially important to note that these experiments always deal with systems of known structure. The experimental challenge is to be able to discern small changes in the relative intensities of the different diffraction

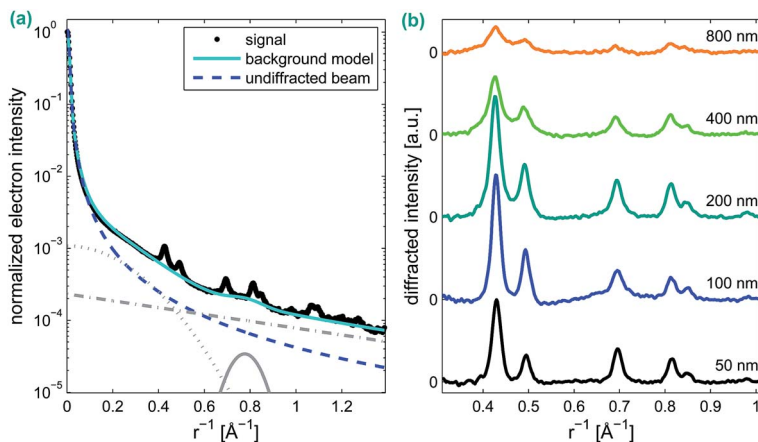


Fig. 6 (a) Example for electron diffraction from poly-crystalline aluminum film after azimuthal integration. The signal (black) has been normalized to the transmitted peak intensity. A reference image including dark current has been subtracted before integration. Further subtraction removes the un-diffracted beam (dashed blue line) and incoherent background (solid blue line) from the coherently diffracted signal. Incoherent contributions are shown in grey. (b) Diffracted intensity after background subtraction. The diffraction patterns are stacked for better visibility.

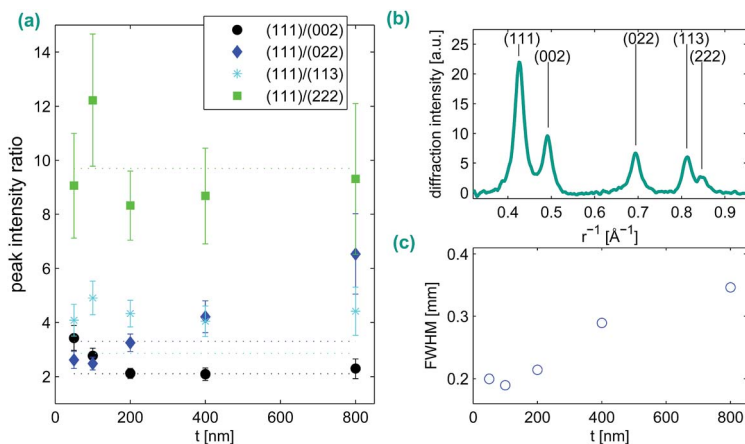


Fig. 7 (a) Ratio of peak intensities in diffraction pattern. The dashed lines gives the scattering ratio for a perfect powder sample in the single scattering regime for comparison. An example diffraction pattern for 200 nm thickness is shown in (b), where the integrated diffraction rings are labeled with Miller indices. (c) Width of rings in diffraction pattern with increasing thickness.

orders. This control study shows that it is possible to extract structural dynamics from samples as thick as several hundred nanometers to micron thickness at this energy range. This feature of relativistic electrons was one of the primary motivations for developing this source as it dramatically increases the ease of sample preparation and opens up solution phase chemistry to atomic inspection, which is much easier to realize with micron scale path lengths as opposed to 100 nm needed for nonrelativistic electron studies.

3 Ultrafast dynamics with REGAE

3.1 Finding $t = 0$

In order to perform time-resolved electron diffraction studies, one needs to characterize the instrument's time resolution. Before such studies can be performed in detail however, the temporal overlap ($t = 0$) between pump and probe, in our case excitation laser and electron pulse, needs to be found. Here, a process that is reversible under photoexcitation is favorable. We used the laser induced plasma formation as a means to determine the electron-laser timing using a copper mesh at the target position with an incident fluence of 14.9 mJ cm^{-2} . Images of the mesh are acquired on the detector in transmission mode. The magnification is close to one, so that the lines with a spacing of $24.5 \text{ }\mu\text{m}$ are not resolved in these images. Similar experiments have been presented in ref. 57. Examples of images prior to and after laser irradiation are shown in Fig. 8(a) and (b). The excitation laser with a width of $500 \text{ }\mu\text{m}$, a wavelength of 800 nm and a pulse width of $\approx 80 \text{ fs}$ induces a plasma in the center of the mesh, from where a charged plume is expelled. The probe electron beam is partially deflected by this spatial gradient in charge, which can be observed as the depleted area in the electron density distribution, as depicted in Fig. 8(b). The electron beam seems to be affected on a smaller area than expected from the laser beam size, which we

interpret as higher order absorption processes in the high intensity center of the laser beam. The higher order multi photon absorption processes lead in turn to a reduction in the effective beam diameter giving rise to the observed effect. The excitation arrival time was varied using a delay stage and a series of shadow images was recorded scanning through the time delay between the laser excitation and electron probe pulses. In order to retrieve $t = 0$ from the shadow images, we analyzed the RMS intensity changes in the central area of the beam. As plotted in Fig. 8(c), we observed a step in the signal, the onset of which is assumed to indicate the zero – time point. Furthermore, we evaluated the width of the differential change in intensity and find a FWHM of 0.9 ps where the changes are occurring fastest in the center of the imaged profile. The result indicates that the electron bunch length is in the sub picosecond range.

3.2 Laser induced structural dynamics of gold

The first structural dynamics at REGAE were observed in a similar geometry to that used for the plasma studies, but under single shot conditions. Free standing membranes of polycrystalline gold were used to observe a laser induced structural change. The membranes with a size of 200 μm by 200 μm were excited one by one with a laser pulse, and the resultant diffraction images were recorded. At a fluence of 150 mJ cm^{-2} and 100 fs pulse duration, the excitation leads to melting and therefore damage of the sample, and is not reversible. For the data presented here, 300 of these membranes fabricated on a chip were used. Again, example images before and after laser irradiation are shown in Fig. 9(a) and (b).

The diffraction image after laser irradiation still exhibits diffraction rings, but the amplitude of the outer rings is diminished. This change indicates a loss of long range order due to melting of the sample. The timescale of this change from ordered to a disordered state is shown in Fig. 9(c). Here, the diffraction rings' amplitudes are plotted *versus* delay time between laser and electron bunch. Each time step was repeated three times. Within five picoseconds after excitation, the outer rings are fading, while the ring indexed with (111) gains in intensity. This gain is attributed to an overlap of the (111) diffraction ring and diffraction from a liquid state. At longer delay times we find the sample completely destroyed. The above results are the first time-resolved studies of REGAE that clearly show its capabilities for single shot structure determination on the 100 fs time scale. The

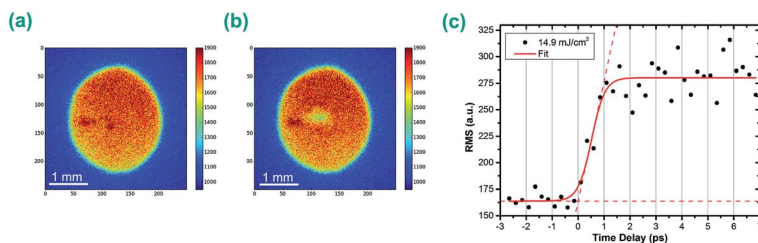


Fig. 8 Shadow images of a copper mesh before (a) and after (b) laser irradiation. The deflection of the electron bunch can be observed as a depleted region in the electron beam profile. The analysis of the signal is shown in (c): the signal RMS in the central region is evaluated and shows a step with a time constant of 0.9 ps.

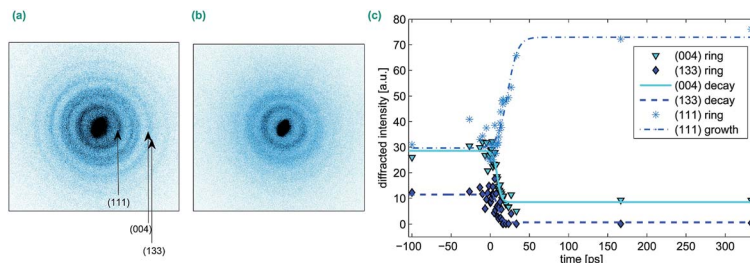


Fig. 9 Single shot diffraction patterns before (a) and after (b) laser excitation. (c) Intensity of the diffraction rings as a function of time delay between pump and probe pulse.

observed dynamics for the particular fluences match very well those found earlier.⁵⁸ The present time resolution is limited by RF timing issues and it must be stated that this limit is primarily due to problems in finding a suitably fast reference system to optimize the phase of the rebunching cavity for optimal compression. The best solution will be to introduce an RF streak camera for enabling optimization of the pulse compression process.⁶² This diagnostic tracks the phase jitter of the RF so it is not suitable for jitter compensation between the RF and the laser excitation. However, by simultaneously recording the central beam position with the high dynamic range detector, it will be possible to achieve an overall time resolution in the 10 fs range, as demonstrated using photo-triggered streak cameras for time stamping and correction of the jitter.^{26–29}

4 Concluding remarks

The present space-time limitations have been increased to the 10 femtosecond time scale with changes in diffraction intensities corresponding to net atomic displacements of less than 0.05 Å with single shot capabilities. This space-time resolution is sufficient now to capture the fastest nuclear motions involved in chemistry. In this respect, the single most restrictive condition on space-time resolution, not discussed within the context of the electron source physics, is the sample constraints. The use of electron structural probes to provide table top high brightness sources by its nature requires very thin samples, on the order of few 10 s of nanometers to 100 nm scale for nonrelativistic electrons. It is the sample limitations that impose the brightness condition in the first place. These are precious samples in which excitation induced damage and thermal effects limiting sampling rate have dictated the need for ultrabright sources. There are some samples however that are just not amenable to such short path lengths. Two prime examples of great interest are solution phase chemistry and protein dynamics. Although, there have been major advances in the development of nanofluidics for this expressed purpose,^{59,60} it is much simpler to use micron scale flow conditions to achieve the desired flow rates for sample exchange. Similarly for protein systems, the highest spatial resolution is achieved in diffraction and the functionally relevant motions involving the protein are spatially distributed leading to very small net RMS atomic motions, yet are central to the proteins role in transducing stored chemical potential into function.⁴ If we are ever to make the key connections between correlated motions inherent to particular protein

structures or motifs as part of a generalized understanding of protein structure–function correlations, we will need to make these observations in diffraction. All protein crystals are water soluble and as such are not amenable to classic microtome methods to fabricate 100 nm thin slices needed for nonrelativistic electron probes. Herein is the major advantage of relativistic electrons over lower energy sources. There are scaling relations for the electron mean free path that indicate higher energy electrons will enable the use of thicker samples. However, the difference inelastic and elastic scattering need to be determined as there are approximations as is evident from the noted differences between experimental measurements and calculated scattering cross-sections. Most important, sample quality has an enormous influence on spatial resolution (*vide infra*). In the present work, we have conducted a systematic study of the effect of sample thickness on the apparent structure resolution. By comparing both experiment and theoretical calculations based on multi-slice methods for dealing with multiple electron scattering, we find that it is possible to use samples up to thicknesses of nearly 1 micron for materials of low Z corresponding to the range of most organic and biological systems of interest. This finding also means that it should be possible to dramatically relax the engineering requirements for introducing flowing liquid cells with electron transparent SiN windows. In terms of spatial resolution limits for discerning structural changes, it is important to emphasize further that the measurement does not have the same requirements as needed to resolve a previously unknown structure. The experiment relies on knowing the initial and in most cases final structure and observing the differential displacements in atomic positions that connect one structure to another. This observation gives us directly information on the key modes coupled to the reaction coordinate and enables observation of the reduction in dimensionality that occurs in curve cross regions between reactant and product surfaces. This feature is central to chemistry and it is this enormous reduction in dimensionality in barrier or curve crossing regions that ultimately makes chemistry a transferable concept. These relatively small but highly correlated motions are observable as long as the relative ratios of the various diffraction orders are conserved and within the dynamic range of the structurally induced changes in intensity. We therefore conclude that it will be possible to pull out the structural changes for many classes of time-resolved diffraction experiments, involving samples that were previously thought intractable due to either their liquid nature or sample thickness issues. This finding that multiple electron scattering is not as big an effect as sample quality and attenuation with sample thickness has enormous implications for improving sample preparation methods. This study also reaffirms the primary motivation for the development of relativistic electron sources for atomically resolved structural dynamics as this source greatly relaxes sample requirements for all classes of study. Future investigations comparing data to calculated diffraction patterns will give more insight into the sensitivity that is required to further confirm our observation.

In terms of space-time resolution, relativistic sources also offer the highest possible source brightness for a given photocathode. The high- Q RF cavities provide the highest possible field gradients to accelerate the electron bunch up to the relativistic regime prior to any excessive space-charge broadening effects can spoil the space time correlation of the electrons in the accelerating field. This condition is central to the use of rebunching cavities to correct the small velocity

spread from the field gradient. As shown in the present work, based largely on well tested simulations, pulses as short as 10 fs with electron bunch charges of 10^6 to 10^7 electrons per pulse for typical matching of electron beam to laser excitation beam parameters are achievable. It should be noted that there is a great deal of effort going into further increasing field gradients for next generation electron accelerators and light sources. The use of extremely high peak power few cycle THz pulses has recently been demonstrated to give uniform acceleration and deceleration of nonrelativistic seed electrons with estimated field gradients in excess of 1 GV m^{-1} or more than an order of magnitude larger than the best RF cavities.⁶¹ This development would lead to correspondingly shorter electron pulses for a given bunch density. With respect to improving time resolution, concepts similar to streaking with RF deflecting structures might be implemented in the future as well.⁶²

The most important advances in electron source brightness will deal with the transverse coherence limitations. The present photocathode typically has initial transverse energy spreads of 0.2 to 0.6 eV. This initial energy spread is the greatest limiting factor in the transverse coherence and ability to image complex molecular systems such as proteins. Even within this range of transverse momentum spread, it has been possible to now track atomic motions for large molecular systems with unit cells of $>3 \text{ nm}$ that are comparable to unit cells of many important protein systems.⁶³ Further decreases in transverse momentum spread will make higher resolution of even minute motions as well as scaling to larger and more complex systems. In this respect, the use of ultracold atom sources using threshold ionization of Rydberg states have given results close to the theoretical quantum limit for fermions with respect to the minimum transverse velocity spread, yielding effective electron temperatures of 10 K or less than 0.6 meV.⁴¹ This approach, however, is limited in electron density by the relatively low atom density achievable in ultracold atom traps. In order to get sufficient electron numbers for near single shot conditions, the initial beam size approaches mm dimensions that cancel the net reduction in emittance. The electron beam is indeed very cold but the angular distribution does not lead to much improvement in the transverse coherence at the sample position due to the very large source size at the photocathode. We contend that the brightest photocathode will still be based on solid state cathodes. Significant progress has been made lately in understanding the scattering issues and boundary conditions for photoemission from solid state systems. Recent studies of trialkali photocathodes have given evidence for thermally limited photoemission with energy spreads of 160 meV at room temperature,⁶⁴ and factors of 10 reduction are clearly possible with excitation closer to threshold. These photocathodes also enjoy relatively high quantum yields as found for other semiconductor photocathodes such as the routinely used Cs_2Te materials. Although it is not straightforward, it should be possible to use cryogenically cooled solid state photocathodes. The challenge is to thermally isolate the cathode section of the electron gun while still having sufficient conduction to avoid excessive charge build up and break down at the high fields used for extraction. It should nevertheless be possible to go to 10 K for suitable source sizes that would give an increase in source brightness of approximately 2 orders of magnitude over the commonly used photocathodes in femtosecond electron diffraction studies. In this event, it will be possible to scale up the

experiments to the study of effectively any molecular system and potentially even biological systems.

The above technical achievements could be made in the relatively short term. As with all experiments aimed at structure determination, the quality of the sample ultimately dictates the limits. Future efforts will need to focus on new methods of introducing samples into the vacuum environment of electron diffraction or real space imaging systems. With the relatively recent advent of nanotechnology into this domain, there is reason to believe that it will soon be possible to introduce large arrays of crystals, with the potential for M-pixel arrays of nanocrystals into the sample chambers. High throughput methods developed for XFEL experiments could also be adopted for electron use with appropriate design of environmental enclosures around the sample viewing area. Ion milling and *in situ* growth of 2D crystals and nanocrystals will need to be explored.¹⁹ In all cases, the lessons learned in increasing source brightness will pay enormous dividends for increasing the spatial resolution using electrons for static structure determinations. In the end, it will be the sample that will dictate the space-time resolution limits – as it should be.

Acknowledgements

We gratefully acknowledge the support received for this collaborative effort by DESY (member of the Helmholtz Association (HGF)), the Max Planck Society, and the Hamburg Centre for Ultrafast Imaging, CUI (DFG-EXC1074). We are indebted to R. Brinkmann and H. Dosch of DESY for supporting this project. Also, we thank Hamburg University (UHH) for supporting the setup of the experiment as well as the MCS, MIN, MKK, MSK, MVS groups of DESY for countless support during setup and experiment. In this respect we particularly like to thank M. Hüning, J. Herrmann, R. Jonas, R. Kammering, T. Kozak, A. Labudda, U. Laustoer, S. Lederer, L. Lilje, D. Lipka, J. Müller, K. Müller, U. Mavric, I. Peperkorn, S. Pfeiffer, H. Schlarb, C. Schmidt, M. Seebach, M. Titberidze, M. Walla, S. Weisse, and K. Witt for great support. T. Hasegawa thanks J. K. Dewhurst for providing EDiCo electron diffraction code and his technical support. We are also grateful for technical support from D. Gitaric and J. Gonschior.

References

- 1 J. C. Polanyi and A. H. Zewail, *Acc. Chem. Res.*, 1995, **28**, 119–132.
- 2 J. R. Dwyer, C. T. Hebeisen, R. Ernstorfer, M. Harb, V. B. Deyirmenjian, R. E. Jordan and R. J. D. Miller, *Philos. Trans. R. Soc., A*, 2006, **364**, 741–778.
- 3 B. J. Siwick, J. R. Dwyer, R. E. Jordan and R. J. D. Miller, *Science*, 2003, **302**, 1382–1385.
- 4 R. J. D. Miller, *Annu. Rev. Phys. Chem.*, 2014, **65**, 583–604.
- 5 M. Gao, C. Lu, H. Jean-Ruel, L. C. Liu, A. Marx, K. Onda, S.-y. Koshihara, Y. Nakano, X. Shao, T. Hiramatsu, G. Saito, H. Yamochi, R. R. Cooney, G. Moriena, G. Sciaini and R. J. D. Miller, *Nature*, 2013, **496**, 343–346.
- 6 M. J. J. Vrakking and T. Elsaesser, *Nat. Photonics*, 2012, **6**, 645–647.
- 7 P. Emma, R. Akre, J. Arthur, R. Bionta, C. Bostedt, J. Bozek, A. Brachmann, P. Bucksbaum, R. Coffee, F.-J. Decker, Y. Ding, D. Dowell, S. Edstrom, A. Fisher, J. Frisch, S. Gilevich, J. Hastings, G. Hays, P. Hering, Z. Huang,

- R. Iverson, H. Loos, M. Messerschmidt, A. Miahnahri, S. Moeller, H.-D. Nuhn, G. Pile, D. Ratner, J. Rzepiela, D. Schultz, T. Smith, P. Stefan, H. Tompkins, J. Turner, J. Welch, W. White, J. Wu, G. Yocky and J. Galayda, *Nat. Photonics*, 2010, **4**, 641–647.
- 8 A. Barty, J. Küpper and H. N. Chapman, *Annu. Rev. Phys. Chem.*, 2013, **64**, 415–435.
- 9 P. Hänggi and M. Borkovec, *Rev. Mod. Phys.*, 1990, **62**, 251–341.
- 10 D. D. Dlott, *J. Opt. Soc. Am. B*, 1990, **7**, 1638–1652.
- 11 R. J. D. Miller, *Annu. Rev. Phys. Chem.*, 1991, **42**, 581–614.
- 12 P. Altoè, A. Cembran, M. Olivucci and M. Garavelli, *PNAS*, 2010, **107**, 20172–20177.
- 13 V. I. Prokhorenko, A. Halpin, P. J. M. Johnson, R. J. D. Miller and L. S. Brown, *J. Chem. Phys.*, 2011, **134**, 085105.
- 14 R. J. D. Miller, *Science*, 2014, **343**, 1108–1116.
- 15 M. Harmand, R. Coffee, M. R. Bionta, M. Chollet, D. French, D. Zhu, D. M. Fritz, H. T. Lemke, N. Medvedev, B. Ziaja, S. Toleikis and M. Cammarata, *Nat. Photonics*, 2013, **7**, 215–218.
- 16 A. Aquila, M. S. Hunter, R. B. Doak, R. a. Kirian, P. Fromme, T. a. White, J. Andreasson, D. Arnlund, S. Bajt, T. R. M. Barends, M. Barthelmess, M. J. Bogan, C. Bostedt, H. Bottin, J. D. Bozek, C. Caleman, N. Coppola, J. Davidsson, D. P. DePonte, V. Elser, S. W. Epp, B. Erk, H. Fleckenstein, L. Foucar, M. Frank, R. Fromme, H. Graafsma, I. Grotjohann, L. Gumprecht, J. Hajdu, C. Y. Hampton, A. Hartmann, R. Hartmann, S. Hau-Riege, G. Hauser, H. Hirsemann, P. Holl, J. M. Holton, A. Hömke, L. Johansson, N. Kimmel, S. Kassemeyer, F. Krasniqi, K.-U. Kühnel, M. Liang, L. Lomb, E. Malmerberg, S. Marchesini, A. V. Martin, F. R. N. C. Maia, M. Messerschmidt, K. Nass, C. Reich, R. Neutze, D. Rolles, B. Rudek, A. Rudenko, I. Schlichting, C. Schmidt, K. E. Schmidt, J. Schulz, M. M. Seibert, R. L. Shoeman, R. Sierra, H. Soltau, D. Starodub, F. Stellato, S. Stern, L. Strüder, N. Timneanu, J. Ullrich, X. Wang, G. J. Williams, G. Weidenspointner, U. Weierstall, C. Wunderer, A. Barty, J. C. H. Spence and H. N. Chapman, *Opt. Express*, 2012, **20**, 2706–2716.
- 17 E. Möhr-Vorobeve, S. L. Johnson, P. Beaud, U. Staub, R. De Souza, C. Milne, G. Ingold, J. Demsar, H. Schaefer and A. Titov, *Phys. Rev. Lett.*, 2011, **107**, 036403.
- 18 A. Zarrine-Afsar, C. Müller, F. O. Talbot and R. J. D. Miller, *Anal. Chem.*, 2011, **83**, 767–773.
- 19 A. Zarrine-Afsar, T. R. M. Barends, C. Müller, M. R. Fuchs, L. Lomb, I. Schlichting and R. J. D. Miller, *Acta Crystallogr., Sect. D: Biol. Crystallogr.*, 2012, **68**, 321–323.
- 20 J. C. H. Spence, U. Weierstall and H. N. Chapman, Reports on progress in physics, *Phys. Soc.*, 2012, **75**, 102601.
- 21 A. H. Zewail, *Annu. Rev. Phys. Chem.*, 2006, **57**, 65–103.
- 22 P. Baum and A. H. Zewail, *Proc. Natl. Acad. Sci. U. S. A.*, 2006, **103**, 16105–16110.
- 23 B. J. Siwick, J. R. Dwyer, R. E. Jordan and R. J. D. Miller, *J. Appl. Phys.*, 2002, **92**, 1643.
- 24 T. van Oudheusden, E. F. de Jong, S. B. van der Geer, W. P. E. M. O. t. Root, O. J. Luiten and B. J. Siwick, *J. Appl. Phys.*, 2007, **102**, 093501.
- 25 L. Veisz, G. Kurkin, K. Chernov, V. Tarnetsky, a. Apolonski, F. Krausz and E. Fill, *New J. Phys.*, 2007, **9**, 451–451.

- 26 M. Gao, H. Jean-Ruel, R. R. Cooney, J. Stampe, M. D. Jong, M. Harb, G. Sciaini, G. Moriena and R. J. D. Miller, *Opt. Express*, 2012, **20**, 799–802.
- 27 R. P. Chatelain, V. R. Morrison, C. Godbout and B. J. Siwick, *Appl. Phys. Lett.*, 2012, **101**, 081901.
- 28 R. P. Chatelain, V. Morrison, C. Godbout, B. van der Geer, M. de Loos and B. J. Siwick, *Ultramicroscopy*, 2012, **116**, 86–94.
- 29 M. Gao, Y. Jiang, G. H. Kassier and R. J. Dwayne Miller, *Appl. Phys. Lett.*, 2013, **103**, 033503.
- 30 T. Elsaesser and M. Woerner, *Acta Crystallogr., Sect. A: Found. Crystallogr.*, 2010, **66**, 168–178.
- 31 V. Juvé, M. Holtz, F. Zamponi, M. Woerner, T. Elsaesser and a. Borgschulte, *Phys. Rev. Lett.*, 2013, **111**, 217401.
- 32 M. Woerner, F. Zamponi, Z. Ansari, J. Dreyer, B. Freyer, M. Prémont-Schwarz and T. Elsaesser, *J. Chem. Phys.*, 2010, **133**, 064509.
- 33 J. B. Hastings, F. M. Rudakov, D. H. Dowell, J. F. Schmerge, J. D. Cardoza, J. M. Castro, S. M. Gierman, H. Loos and P. M. Weber, *Appl. Phys. Lett.*, 2006, **89**, 184109.
- 34 P. Musumeci, J. T. Moody, C. M. Scoby, M. S. Gutierrez and M. Westfall, *Appl. Phys. Lett.*, 2010, **97**, 063502.
- 35 R. Li, W. Huang, Y. Du, L. Yan, Q. Du, J. Shi, J. Hua, H. Chen, T. Du, H. Xu and C. Tang, *Rev. Sci. Instrum.*, 2010, **81**, 036110.
- 36 P. Musumeci, J. T. Moody, C. M. Scoby, M. S. Gutierrez, M. Westfall and R. K. Li, *J. Appl. Phys.*, 2010, **108**, 114513.
- 37 C. M. Scoby, P. Musumeci, J. T. Moody and M. S. Gutierrez, *Phys. Rev. Spec. Top.-Accel. Beams*, 2010, **13**, 022801.
- 38 Y. Murooka, N. Naruse, S. Sakakihara, M. Ishimaru, J. Yang and K. Tanimura, *Appl. Phys. Lett.*, 2011, **98**, 251903.
- 39 A. M. Michalik, E. Y. Sherman and J. E. Sipe, *J. Appl. Phys.*, 2008, **104**, 054905.
- 40 G. Sciaini and R. J. D. Miller, *Rep. Prog. Phys.*, 2011, **74**, 096101.
- 41 W. J. Engelen, M. a. van der Heijden, D. J. Bakker, E. J. D. Vredenburg and O. J. Luiten, *Nat. Commun.*, 2013, **4**, 1693.
- 42 A. Rother and K. Scheerschmidt, *Ultramicroscopy*, 2009, **109**, 154–160.
- 43 L. Reimer and H. Kohl, *Transmission Electron Microscopy*, Springer, 2008.
- 44 K. Dewenhurst and D. Rankin, *EDICo – Electron diffraction code*, <http://edico.sourceforge.net/>.
- 45 R. F. Egerton, *Phys. Status Solidi A*, 1976, **663**, 663–668.
- 46 B. Kabius, P. Hartel, M. Haider, H. Müller, S. Uhlemann, U. Loebau, J. Zach and H. Rose, *J. Electron Microsc.*, 2009, **58**, 147–155.
- 47 CST STUDIO SUITE, CST Computer Simulation Technology AG, <http://www.cst.com>.
- 48 M. Reiser, *Theory and Design of Charged Particle Beams*, Wiley, 2nd edn, 2008.
- 49 R. K. Li and P. Musumeci, *Phys. Rev. Applied*, 2014, **2**, 024003.
- 50 D. Xiang, F. Fu, J. Zhang, X. Huang, L. Wang, X. Wang and W. Wan, *Nucl. Instrum. Methods Phys. Res., Sect. A*, 2014, **759**, 74–82.
- 51 H. Delsim-Hashemi and K. Flöttmann, *Proceedings of IPAC2014*, Dresden, Germany, 2014.
- 52 D. Lipka and M. Seebach, *Proceedings of IBIC2013*, 2013, pp. 872–875.
- 53 S. Bayesteh and K. Floettmann, *Proceedings of IPAC2014*, Dresden, Germany, 2014, pp. 3515–3517.

- 54 M. Hoffmann, H. Kay, U. Mavric, H. Schlarb, C. Schmidt, W. Jalmuzna, T. Kozak and A. Piotrowski, *Proceedings of IPAC2013*, Shanghai, China, 2013, pp. 2938–2940.
- 55 K. Floettmann, *ASTRA - A Space Charge Tracking Algorithm*, <http://www.desy.de/mpyflo/>, 1997–2014.
- 56 CrystalMaker Software Ltd, <http://www.crystallmaker.com>.
- 57 C. M. Scoby, R. K. Li and P. Musumeci, *Ultramicroscopy*, 2013, **127**, 14–18.
- 58 R. Ernstorfer, M. Harb, C. T. Hebeisen, G. Sciaini, T. Dartigalongue and R. J. D. Miller, *Science*, 2009, **323**, 1033–1037.
- 59 J. M. Grogan, N. M. Schneider, F. M. Ross and H. H. Bau, *J. Indian Inst. Sci.*, 2012, **92**, 295.
- 60 C. Mueller, M. Harb, J. R. Dwyer and R. J. D. Miller, *J. Phys. Chem. Lett.*, 2013, **4**, 2339–2347.
- 61 S. Carbajo, L. Wong, E. Nanni, R. Miller and F. Kärtner, in *Frontiers in Optics*, 2014, OSA Technical Digest, <http://dx.doi.org/10.1364/FIO.2014.FTh2A.2>.
- 62 K. Floettmann and V. V. Paramonov, *Phys. Rev. ST Accel. Beams*, 2014, **17**, 024001.
- 63 S. Hayes, 2014, in preparation.
- 64 L. Cultrera, I. Bazarov, A. Bartnik, B. Dunham, S. Karkare, R. Merluzzi and M. Nichols, *Appl. Phys. Lett.*, 2011, **99**, 152110.